Plasma Sources Science and Technology

PAPER

Electron heating and control of ion properties in capacitive discharges driven by customized voltage waveforms

To cite this article: A Derzsi *et al* 2013 *Plasma Sources Sci. Technol.* **22** 065009

Plasma Sources Sci. Technol. **22** (2013) 065009 (13pp) doi:10.1088/0963-0252/22/6/065009

Electron heating and control of ion properties in capacitive discharges driven by customized voltage waveforms

A Derzsi[1], I Korolov[1], E Schüngel[2], Z Donkó[1] and J Schulze[2]

[1] Institute for Solid State Physics and Optics, Wigner Research Centre for Physics, Hungarian Academy of Sciences, 1121 Budapest, Konkoly-Thege Miklós str. 29-33, Hungary
[2] Institute for Plasma and Atomic Physics, Ruhr University Bochum, 44780 Bochum, Germany

E-mail: derzsi.aranka@wigner.mta.hu

Received 8 April 2013, in final form 31 July 2013
Published 11 November 2013
Online at stacks.iop.org/PSST/22/065009

Abstract
We investigate the electron heating dynamics in capacitively coupled radio frequency plasmas driven by customized voltage waveforms and study the effects of modifying this waveform and the secondary electron emission coefficient of the electrodes on the spatio-temporal ionization dynamics by particle-in-cell simulations. We demonstrate that changes in the electron heating dynamics induced by voltage waveform tailoring strongly affect the dc self-bias, the ion flux, Γ_i, and the mean ion energy, $\langle E_i \rangle$, at the electrodes. The driving voltage waveform is customized by adding N consecutive harmonics ($N \leqslant 4$) of 13.56 MHz with specific harmonics' amplitudes and phases. The total voltage amplitude is kept constant, while modifying the number of harmonics and their phases. In an argon plasma, we find a dc self-bias, η, to be generated via the electrical asymmetry effect for $N \geqslant 2$. η can be controlled by adjusting the harmonics' phases and is enhanced by adding more consecutive harmonics. At a low pressure of 3 Pa, the discharge is operated in the α-mode and $\langle E_i \rangle$ can be controlled by adjusting the phases at constant Γ_i. The ion flux can be increased by adding more harmonics due to the enhanced electron-sheath heating. $\langle E_i \rangle$ does not remain constant as a function of N at both electrodes due to a change in η. These findings verify previous results of Lafleur *et al*. At a high pressure of 100 Pa and using a high secondary electron emission coefficient of $\gamma = 0.4$, the discharge is operated in the γ-mode and mode transitions are induced by changing the driving voltage waveform. Due to these mode transitions and the specific ionization dynamics in the γ-mode, Γ_i is no longer constant as a function of the harmonics' phases and decreases with increasing N.

(Some figures may appear in colour only in the online journal)

1. Introduction

Capacitively coupled radio frequency (CCRF) discharges are irreplaceable tools for surface processing applications such as plasma-enhanced chemical vapor deposition (PECVD) and plasma etching. These techniques are the basis for the manufacturing of many high technology products such as integrated circuits, solar cells and biocompatible surfaces [5–7]. Moreover, atmospheric pressure capacitive micro-discharges are frequently used for biomedical applications such as sterilization [8–15]. In order to optimize these applications specific flux-energy distribution functions (FEDF) of different species (electrons, ions, neutrals) are required at the surface to be processed and in the plasma bulk. The shape of these FEDFs is determined by complex particle heating and transport dynamics in the plasma, which are not fully understood and, thus, typically cannot be controlled.

Different electron heating mechanisms, such as stochastic and ohmic heating, are known [5, 16–27]. Depending on the choice of global control parameters, e.g. neutral gas pressure and driving voltage amplitude, different modes of discharge operation, such as the α- [28], γ- [28, 29] or the Ω-mode [12, 31–38], have been identified in single-frequency plasmas based on the above-mentioned mechanisms of electron heating.

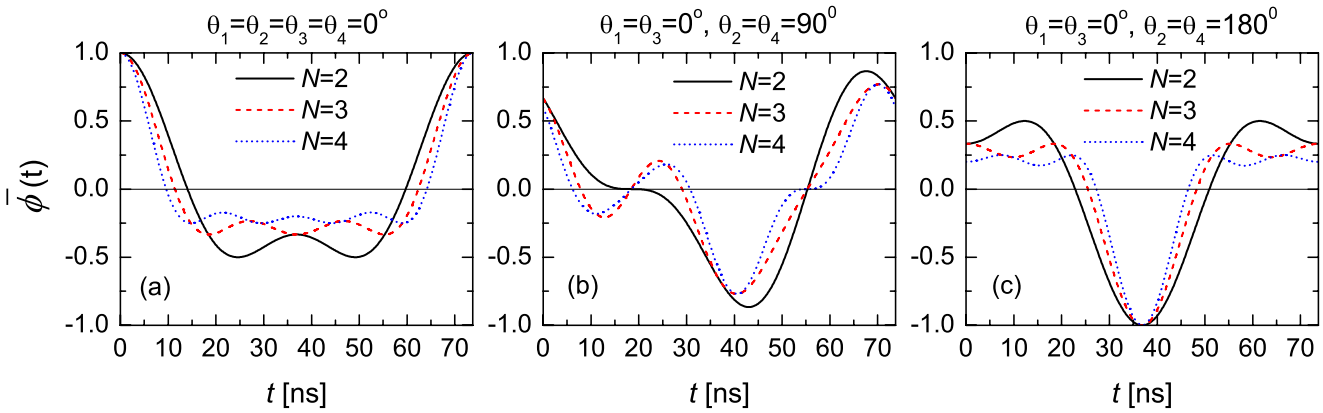

Figure 1. Normalized driving voltage waveform, $\bar{\phi}(t) = \phi(t)/\phi_{\mathrm{tot}}$, for exemplary choices of N and θ_k.

The electron heating mode and transport determines the shape of the electron energy distribution function (EEDF) at different positions in the plasma and times within the RF period. The shape of the EEDF in turn determines the ionization and dissociation dynamics. Ions and neutral radicals generated in the plasma bulk are transported towards the boundary surfaces. Positive ions are strongly accelerated by the electric field inside the sheaths. Finally, process relevant FEDFs are formed at the boundary surfaces.

Applications are typically optimized empirically rather than based on a detailed understanding of the complex plasma physics. Methods to customize FEDFs at the boundary surfaces are mostly limited to controlling integral quantities such as the total flux, Γ_x, and the mean energy, $\langle E_x \rangle$, of species x. The shape of the ion FEDF at boundary surfaces has been customized by arbitrary substrate biasing in high-density remote sources such as inductively coupled or helicon plasmas [39–41].

In single-frequency electropositive CCRF plasmas, the ion flux, Γ_{i}, and the mean ion energy, $\langle E_{\mathrm{i}} \rangle$, cannot be controlled separately [42]. As this separate control is important for many applications, classical dual-frequency discharges, operated at two substantially different frequencies, have been developed [43–45]. Within narrow process windows, i.e. specific choices of pressure, power and electrode material, $\langle E_{\mathrm{i}} \rangle$ is mainly controlled by the low-frequency (lf) voltage amplitude, while Γ_{i} is controlled by the high-frequency (hf) voltage amplitude. This separate control is, however, strongly limited by the frequency coupling [13–15, 29, 30, 46, 47] and the effect of secondary electrons [29, 48]. The frequency coupling in classical dual-frequency CCPs has been found to be affected by the phase between the driving voltage waveforms [14, 30].

Significantly better separate control can be realized in CCRF discharges driven by multiple consecutive harmonics based on the electrical asymmetry effect (EAE) [49–54], i.e. by applying the following voltage waveform, $\phi(t)$, to one electrode:

$$\phi(t) = \sum_{k=1}^{N} \phi_k \cos\left(2\pi k f t + \theta_k\right) \qquad \text{with} \quad \phi_{\mathrm{tot}} = \sum_{k=1}^{N} \phi_k. \tag{1}$$

Here, N is the total number of consecutive harmonics, k is an integer number and f is the fundamental frequency. ϕ_k is the amplitude and θ_k is the fixed, but adjustable phase of the kth harmonic. ϕ_{tot} is the total applied voltage amplitude. Figure 1 shows representative examples of the normalized driving voltage waveform, $\bar{\phi}(t) = \phi(t)/\phi_{\mathrm{tot}}$, for $f = 13.56\,\mathrm{MHz}$ and specific values of N as well as θ_k. The symmetry of such a plasma can be quantified by the symmetry parameter, ε [51]:

$$\varepsilon = \left|\frac{\hat{\phi}_{\mathrm{sg}}}{\hat{\phi}_{\mathrm{sp}}}\right| \approx \left(\frac{A_{\mathrm{p}}}{A_{\mathrm{g}}}\right)^2 \frac{\bar{n}_{\mathrm{sp}}}{\bar{n}_{\mathrm{sg}}} \left(\frac{Q_{\mathrm{mg}}}{Q_{\mathrm{mp}}}\right)^2. \tag{2}$$

Here, $\hat{\phi}_{\mathrm{sg}}$ and $\hat{\phi}_{\mathrm{sp}}$ are the maximum voltage drops across the sheath at the grounded and powered electrodes, respectively. $\bar{n}_{\mathrm{sg}}$ and $\bar{n}_{\mathrm{sp}}$ are the spatially averaged ion densities, and Q_{mg} and Q_{mp} are the positive space charges in the respective sheath at the time of maximum sheath voltage at the grounded and powered electrodes, respectively. A_{p} and A_{g} are the surface areas of the respective electrodes. The discharge will be symmetric, if $\varepsilon = 1$.

According to an analytical model described in detail in [51] a dc self-bias, η, is generated in CCRF discharges:

$$\eta \approx -\frac{\phi_{\mathrm{m1}} + \varepsilon\phi_{\mathrm{m2}}}{1+\varepsilon}. \tag{3}$$

Here, ϕ_{m1} and ϕ_{m2} are the applied voltages at the time of maximum sheath voltage at the grounded and powered electrodes, respectively. In low-pressure single-frequency electropositive plasmas, these times uniquely correspond to the times of maximum and minimum applied voltage, respectively. In multi-frequency plasmas, however, depending on the choices of ϕ_k and θ_k there can be multiple global extrema of the driving voltage waveform (see figure 1), so that it is important to use the driving voltages at the times of maximum sheath voltage in equation (3).

Previous investigations of the EAE yielded the following main results: if the discharge is symmetric ($\varepsilon = 1$), a dc self-bias will be generated, if the absolute values of ϕ_{m1} and ϕ_{m2} are different. This difference and, thus, η can be controlled via the harmonics' phases and can be increased by adding more consecutive harmonics with specific amplitudes defined by the following criterion to the driving voltage waveform [54]:

$$\phi_k = \phi_0 \frac{N-k+1}{N} \qquad \text{with} \quad \phi_0 = \frac{2\phi_{\mathrm{tot}}}{N+1}. \tag{4}$$

The choices of the total applied voltage amplitude, ϕ_{tot}, and the number of applied consecutive harmonics determine the ion flux and the absolute values of the mean ion energies at the electrodes.

In dual-frequency discharges operated at 13.56 and 27.12 MHz in the α-mode, $\langle E_i \rangle$ can be controlled efficiently by adjusting the phase between both harmonics, while Γ_i remains constant, since the voltage amplitudes are not changed [51]. Reducing the fundamental driving frequency results in a lower dc self-bias and a less efficient control of $\langle E_i \rangle$ [55]. In electrically asymmetric plasmas, Γ_i can be controlled by adjusting the harmonics' amplitudes. However, changing the voltage amplitudes also affects the sheath voltages and, therefore, $\langle E_i \rangle$, so that the ion flux cannot be controlled at a constant mean ion energy in this way.

Recently, Lafleur *et al* found experimentally [1, 4] that Γ_i can be increased by adding more consecutive harmonics, i.e. by increasing N, at low and almost constant $\langle E_i \rangle$ at the grounded electrode, while keeping the peak-to-peak voltage of the waveform constant. The increase in Γ_i as a function of N has been explained by enhanced stochastic sheath heating in the α-mode by adding higher harmonics. By particle-in-cell (PIC) simulations, assuming specific electrode materials with low γ-coefficients, they showed [2, 3] that a similar effect can be realized by using repetitive Gaussian pulses and changing their width. Lafleur *et al* investigated argon discharges driven at peak-to-peak voltages between 100 V and 735 V at pressures ranging from about 3 Pa to 65 Pa [1–4].

These results are important, since they provide a method to increase the throughput of large-area PECVD by increasing the ion flux, while avoiding parasitic damage of the deposited layers by energetic ions [56–59]. Such an energetic ion bombardment has been a strong process limitation in large-area CCRF discharges, which are inherently geometrically symmetric, so that the ion bombardment energy at the substrate cannot be reduced by a geometrically induced dc self-bias.

However, previous investigations have been limited to the α-mode operation of CCRF plasmas. Generally, a systematic investigation of the electron heating dynamics in multi-frequency CCRF plasmas operated at more than two consecutive harmonics has never been performed and, correspondingly, the effect of these dynamics and heating mode transitions on the control of ion properties via the EAE has not been quantified. Thus, the following important questions have not yet been answered for CCRF plasmas driven at more than two consecutive harmonics:

- What is the effect of modifying the driving voltage waveform by adding more consecutive harmonics and changing the harmonics' phases on the electron heating and ionization dynamics?
- How does the presence of an electron heating mode different from the α-mode, e.g. the γ-mode, affect the control of ion properties?

These questions are most important for applications using different electrode materials such as large-area PECVD, RF sputtering and plasma etching, which can potentially be improved by the EAE using multiple consecutive harmonics [60]. They are also highly relevant for fundamental research on electron heating in multi-frequency capacitively coupled plasmas.

Here, for the first time we perform a systematic investigation of the electron heating dynamics in CCRF discharges operated at multiple consecutive harmonics ($N > 2$) by PIC simulations to clarify the above questions. Our most important findings are as follows:

- Transitions of the electron heating mode from the α- to the γ-mode induced by changing the driving voltage waveform, pressure and γ strongly affect the control of ion properties at the electrodes.
- At low pressures and high voltages, $\langle E_i \rangle$ can be controlled efficiently by adjusting the harmonics' phases at constant Γ_i via the EAE. The ion flux can be increased by adding higher harmonics to the driving voltage waveform, but $\langle E_i \rangle$ does not remain constant at any electrode under these conditions.
- At a high pressure of 100 Pa and high γ, the mean ion energy can be adjusted via the harmonics' phases, but the ion flux does not remain constant. Adding higher harmonics to the driving waveform results in a decrease in Γ_i under these conditions and $\langle E_i \rangle$ does not remain constant as a function of N.

We explain these findings based on a detailed analysis of the spatio-temporal electron heating and ionization dynamics in multi-frequency CCRF plasmas.

The paper is structured in the following way: this introduction is followed by a description of the PIC simulation used in this work and the discharge conditions investigated. In section 3, the results are presented. This section is split into two parts according to the two different pressures investigated (3 Pa and 100 Pa). Conclusions are drawn in section 4.

2. The simulation method (PIC)

The simulation results presented here are based on a one-dimensional (1d3v) bounded plasma PIC code complemented with a Monte Carlo treatment of collision processes (PIC/MCC). The neutral gas temperature is taken to be $T_g = 400$ K and the electrode gap is $L = 3$ cm for all conditions investigated. The discharge is operated in argon. The cross sections for electron–neutral and ion–neutral collision processes are taken from [61–63]. At the planar, parallel and infinite electrodes, electrons are reflected with a probability of 20% [64]. The ion-induced secondary electron emission coefficient is identical at both electrodes and is varied between 0 and 0.4 to study the effect of γ-electrons on the ionization dynamics and the separate control of ion properties. About 10^5 superparticles of both charged species are used in the simulations, with time steps between 2.5×10^{-12} and 9.2×10^{-12} s, and 300–600 grid points. Simulations are performed at neutral gas pressures of 3 Pa ($\phi_{tot} = 800$ V) and 100 Pa ($\phi_{tot} = 120$ V) to investigate the nearly collisionless low-pressure regime, where stochastic electron heating is dominant (α-mode), and the collisional high-pressure regime,

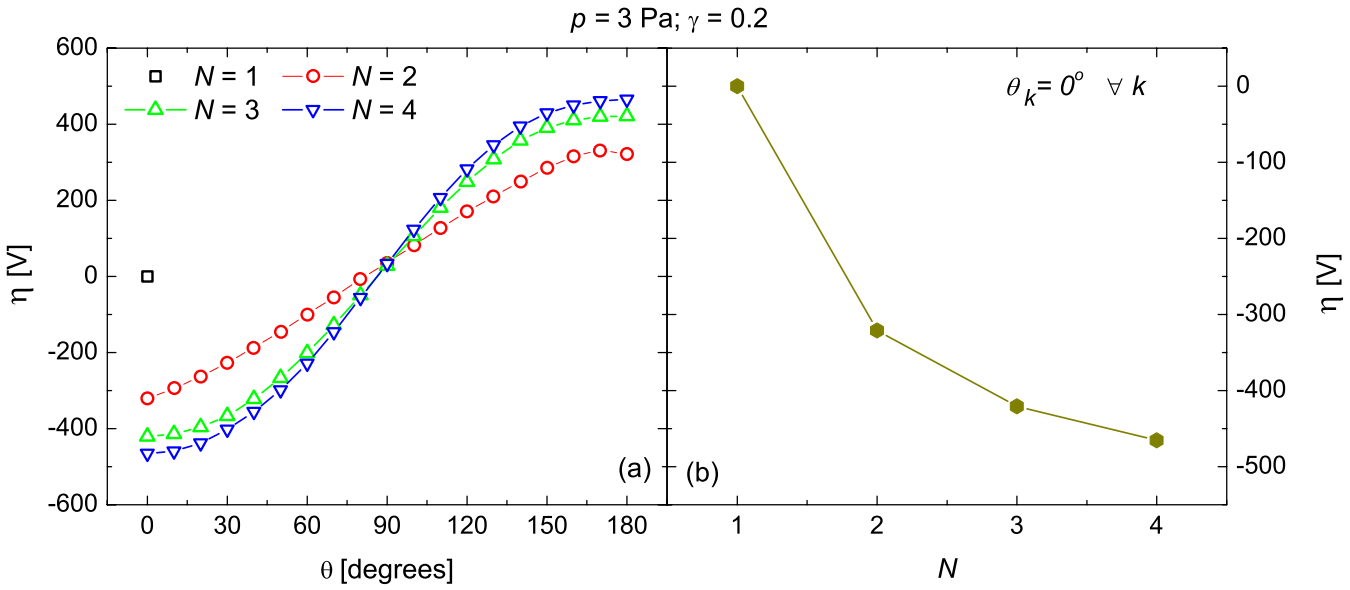

Figure 2. Dependence of the self-bias voltage, η, on (a) the identical phase angle of the even harmonics ($\theta = \theta_2 = \theta_4$, $\theta_1 = \theta_3 = 0°$) for different numbers of applied harmonics, N, and (b) the number of applied harmonics for $\theta_k = 0° \,\forall\, k$ ($p = 3$ Pa, $\phi_{tot} = 800$ V, $\gamma = 0.2$).

where the discharge is operated in the γ-mode for high secondary electron emission coefficients. A voltage waveform corresponding to equation (1) with $f = 13.56$ MHz is applied to one electrode, while the other is grounded. The number of consecutive harmonics, N, is set between 1 and 4; the phases of the even harmonics (θ_2, θ_4) are varied from 0° to 180°. These two phases are chosen to be identical, i.e. $\theta_2 = \theta_4$, while the phases of the odd harmonics are set to 0°, i.e. $\theta_1 = \theta_3 = 0°$. This procedure is based on previous results, which demonstrated that the dc self-bias, η, and the mean ion energies at both electrodes can be changed from their maximum to their minimum by only adjusting the phases of the even harmonics [54].

In the simulations, η is determined in an iterative way to ensure that the charged particle fluxes to each of the two electrodes, averaged over one period of the fundamental frequency, balance. Details of the PIC simulation can be found elsewhere [65].

3. Results

3.1. Low pressure (3 Pa): α-mode

Figure 2(a) shows the dc self-bias, η, as a function of the identical phase angle of the even harmonics ($\theta = \theta_2 = \theta_4$, $\theta_1 = \theta_3 = 0°$) for different numbers of applied harmonics, N. The pressure is 3 Pa, the harmonics' amplitudes are chosen according to equation (4) with $\phi_{tot} = 800$ V, and $\gamma = 0.2$. Adding more consecutive harmonics, i.e. increasing N, enhances the control interval of η [1–4, 54]. Increasing N particularly results in a strong increase in $|\eta|$ at $\theta = 0°$, 180°, which saturates for large N [54]. The dependence of η on N for $\theta = 0°$ is shown as an example in figure 2(b).

Changing $\eta = |\langle\phi_{sg}\rangle| - |\langle\phi_{sp}\rangle|$ corresponds to controlling the difference between the time-averaged sheath voltages, $\langle\phi_{sg}\rangle$ and $\langle\phi_{sp}\rangle$, at the grounded and powered electrodes. Thus, the mean ion energy at the electrodes can be controlled efficiently by adjusting θ, as shown in figures 3(a) and (c). $\langle E_i\rangle$ can be changed by a factor of about 7 under these conditions. As adding more consecutive harmonics to the driving voltage waveform causes $|\eta|$ to increase, the mean ion energy also depends on N. Figures 3(b) and (d) show a significant decrease in $\langle E_i\rangle$ by a factor of about 4 at the grounded electrode and an increase by a factor of about 1.75 at the powered electrode for $\theta_k = 0° \,\forall\, k$. The absolute increase/decrease in $\langle E_i\rangle$ is about 150 eV at both electrodes. These results are qualitatively similar to the observations of Lafleur *et al* [2]. In agreement with them we explain the change in $\langle E_i\rangle$ at both electrodes by (i) a decrease in the sheath width at both electrodes as a function of N due to a higher plasma density caused by an enhanced sheath heating of electrons at higher harmonics and (ii) a more negative dc self-bias at higher N. While a smaller and less collisional sheath causes $\langle E_i\rangle$ to increase at both electrodes, a more negative self-bias causes the mean ion energy to decrease at the grounded electrode and to increase at the powered electrode at $\theta_k = 0° \,\forall\, k$. While these two effects can compensate each other at low driving voltages at the grounded electrode and lead to a constant mean ion energy as a function of N, this is not the case at high driving voltages, as used in this work. Here, the strong increase in $|\eta|$ as a function of N (see figure 2(b)) by about 470 V from $N = 1$ to $N = 4$ dominates and causes $\langle E_i\rangle$ to decrease as a function of N at the grounded electrode.

Figure 4 shows the sheath widths at the powered electrode, s_p, and at the grounded electrode, s_g, as a function of time within one fundamental RF period for $N = 1$ and 4 at $\theta_k = 0° \,\forall\, k$. In the simulations, the sheath widths are determined based on a criterion used by Brinkmann [66]. The maximum sheath widths are identical at both electrodes for $N = 1$ and decrease as a function of N. This decrease is less pronounced at the powered compared with the grounded electrode. There are two mechanisms causing this decrease at both electrodes:

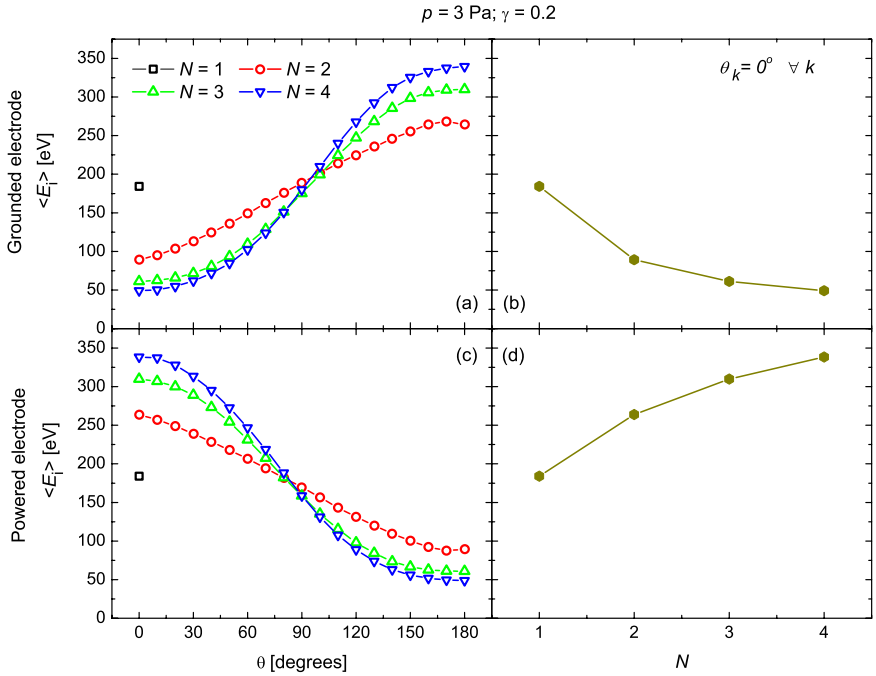

Figure 3. Mean ion energy, $\langle E_\mathrm{i}\rangle$, at the grounded and powered electrodes (top and bottom panels, respectively) as a function of $\theta = \theta_2 = \theta_4$ (left panels) for different number of applied harmonics, N, and as a function of N at $\theta_k = 0^\circ\,\forall\,k$ (right panels); $p = 3$ Pa, $\phi_\mathrm{tot} = 800$ V, $\gamma = 0.2$.

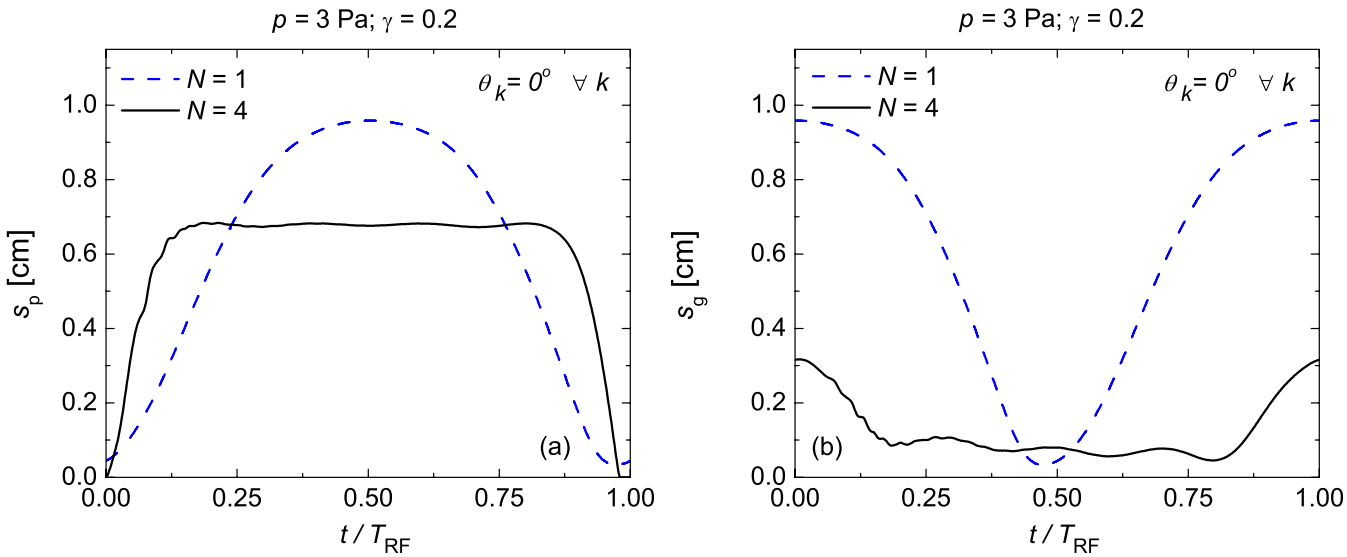

Figure 4. Sheath width at the powered (left plot) and grounded (right plot) electrode as a function of time within one fundamental RF period for $N = 1$ and 4 ($\theta_k = 0^\circ\,\forall\,k$, $p = 3$ Pa, $\phi_\mathrm{tot} = 800$ V, $\gamma = 0.2$).

(i) the plasma density is increased as a function of N. This causes the sheath width to decrease at both sides. (ii) $\bar{n}_\mathrm{sp}$ and $\bar{n}_\mathrm{sg}$ become different at low pressures due to the self-amplification of the EAE [50, 51], i.e. a finite self-bias causes positive ions to be accelerated to higher velocities in one sheath compared with the other. Due to flux continuity the ion density decreases more strongly towards the electrode in one compared with the other sheath. For $\eta < 0$ V this causes $\bar{n}_\mathrm{sp} < \bar{n}_\mathrm{sg}$ and $\varepsilon < 1$ according to equation (2), and a larger maximum sheath voltage at the powered electrode (left plot of figure 5). Thus, the sheath is larger at the powered compared with the grounded electrode for a given total driving voltage amplitude. These two effects counteract at the powered electrode and interfere constructively at the grounded electrode for $\theta_k = 0^\circ\,\forall\,k$, so that the maximum sheath width is smaller at the grounded electrode.

According to the left plot of figure 5, ε is identical to $\bar{n}_\mathrm{sp}/\bar{n}_\mathrm{sg}$ in a single-frequency discharge, but significantly differs from this density ratio for high values of N and $\theta_k = 0^\circ\,\forall\,k$. According to equation (2) this difference is caused by different values of the positive space charge in each sheath at the time of maximum sheath voltage, i.e. $(Q_\mathrm{mg}/Q_\mathrm{mp})^2 \neq 1$. The right plot of figure 5 shows that this factor indeed increases as a function of N. This increase is caused by the following

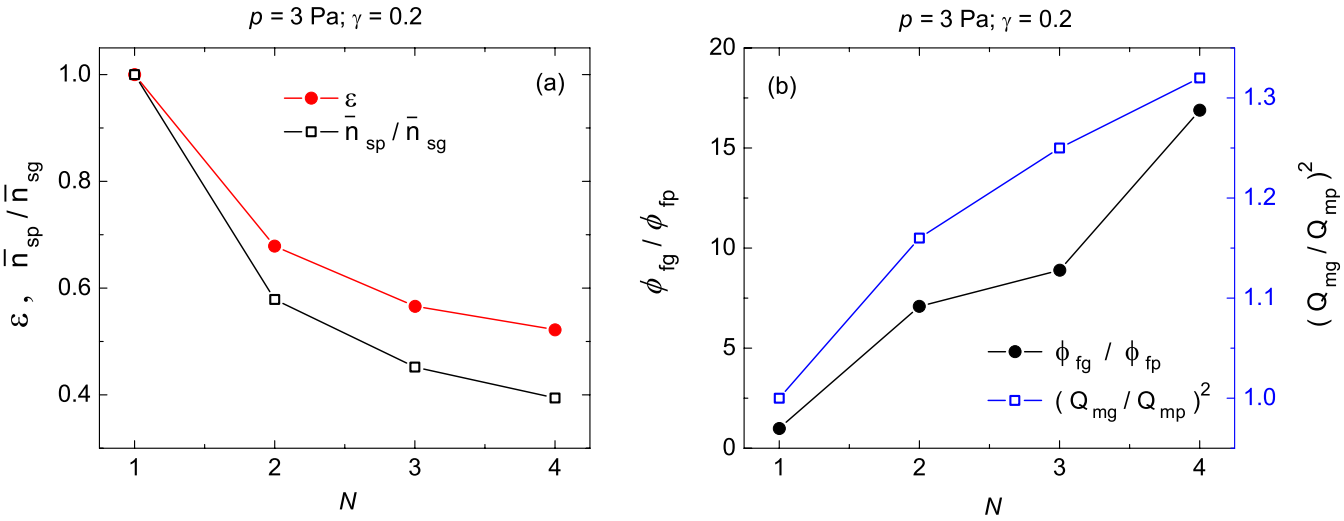

Figure 5. Left: symmetry parameter and $\bar{n}_{sp}/\bar{n}_{sg}$ as a function of N. Right: ratio of the floating potentials and $(Q_{mg}/Q_{mp})^2$ as a function of N ($\theta_k = 0^\circ\,\forall\,k$, $p = 3$ Pa, $\phi_{tot} = 800$ V, $\gamma = 0.2$).

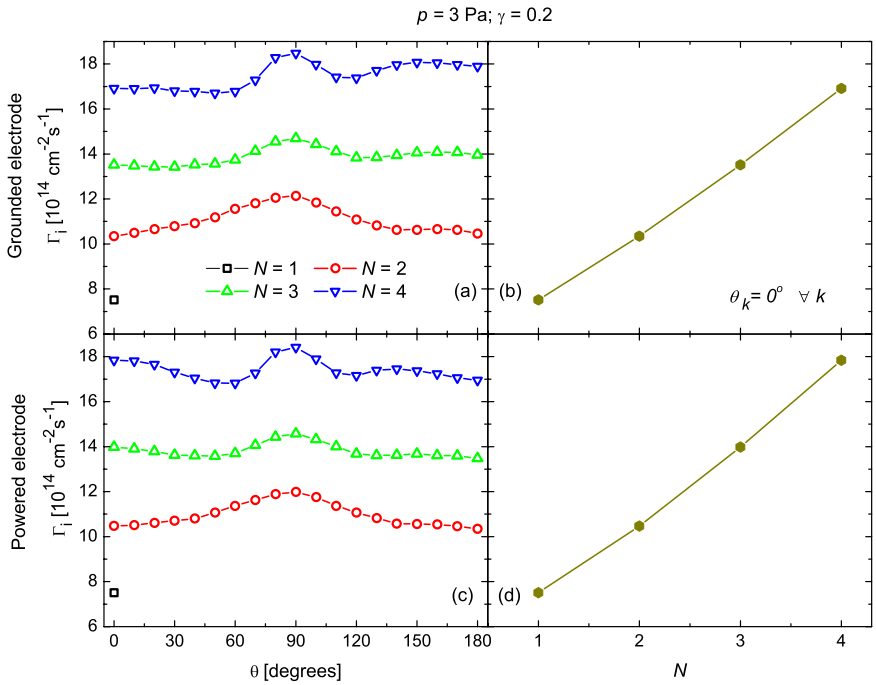

Figure 6. Ion flux, Γ_i, at the grounded and powered electrodes (top and bottom panels, respectively) as a function of $\theta = \theta_2 = \theta_4$ (left panels) for different numbers of applied harmonics, N, and as a function of N at $\theta_k = 0^\circ\,\forall\,k$ (right panels); $p = 3$ Pa, $\phi_{tot} = 800$ V, $\gamma = 0.2$.

mechanism uniquely present in multi-frequency discharges: for $\theta_k = 0^\circ\,\forall\,k$, increasing N causes the sheath to be collapsed for a longer fraction of the fundamental RF period at the grounded compared with the powered electrode (see figure 4). In order to ensure a balance of electron and ion fluxes at this electrode on time average, the minimum sheath voltage at the grounded electrode, i.e. the floating potential, ϕ_{fg}, must increase relative to the floating potential at the powered electrode, ϕ_{fp}. This is also shown in the right plot of figure 5. When the sheath at the powered electrode is collapsed, almost no residual charge is located in this sheath and essentially all uncompensated charge, Q_{tot}, is located inside the grounded sheath. However, when the sheath at the grounded electrode is collapsed, a significant residual charge is located in this sheath and less than Q_{tot} is located inside the powered sheath. Thus, $Q_{mg}/Q_{mp} > 1$ for high values of N at $\theta_k = 0^\circ\,\forall\,k$.

The ion flux remains essentially constant as a function of θ independent of the choice of N at both electrodes (see figures 6(a) and (c)). Thus, $\langle E_i \rangle$ can be controlled separately from Γ_i by adjusting θ as shown in figure 3. Γ_i significantly increases as a function of N at both electrodes (see figures 6(b) and (d)). As $\langle E_i \rangle$ changes significantly as a function of N at both electrodes under these conditions (see figures 3(b), (d)), Γ_i cannot be controlled separately from $\langle E_i \rangle$ by adjusting N. For high values of N, Γ_i is slightly higher at the powered compared with the grounded electrode (18×10^{14} cm^{-2} s^{-1} versus 17×10^{14} cm^{-2} s^{-1}). Such a difference of the ion fluxes at both electrodes has been observed in experiments and in

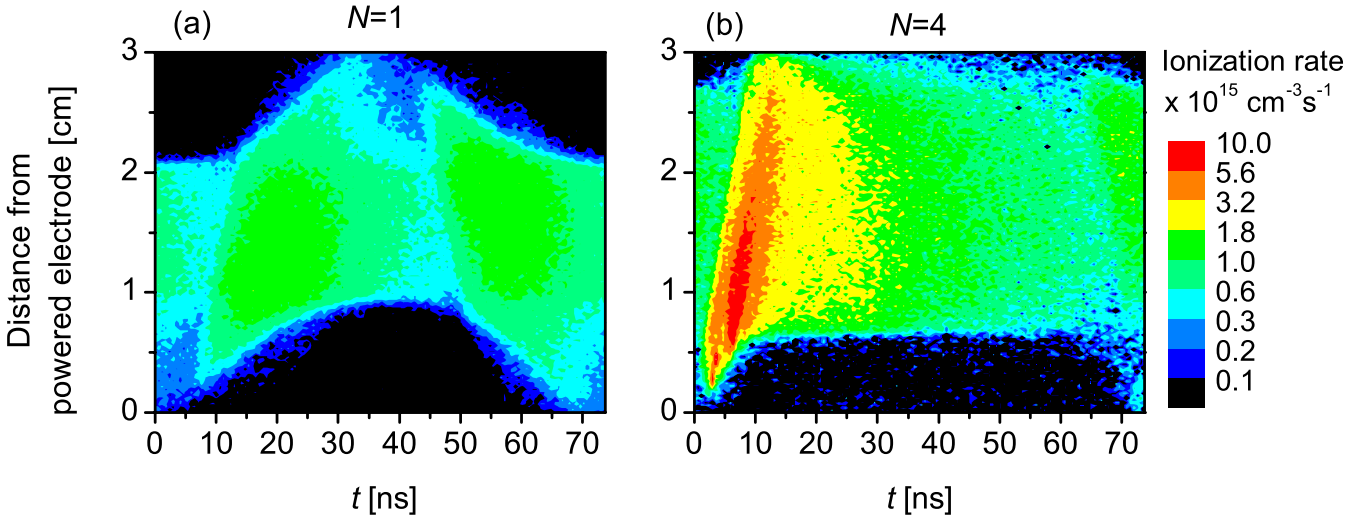

Figure 7. Spatio-temporal plots of the ionization rate for different numbers of applied harmonics, $\theta_k = 0^\circ \forall k$ ($p = 3$ Pa, $\phi_{\text{tot}} = 800$ V, $\gamma = 0.2$). The color scales are logarithmic.

simulations of Lafleur *et al* [1, 2]. They found that the ratio of the fluxes to each electrode increases both by decreasing the width of the applied Gaussian pulse as well as by rising the pressure [2]. They explained this effect by the asymmetric ionization produced by the enhanced electron-sheath heating that induces more ionization at the side where a larger voltage drop occurs (at the powered electrode).

This difference and the increase in Γ_i as a function of N is understood based on the spatio-temporal ionization dynamics for different numbers of consecutive harmonics and for $\theta_k = 0^\circ \forall k$ (figure 7). Due to the low pressure of 3 Pa the discharge is operated in the α-mode, where ionization due to sheath expansion heating of electrons dominates [28]. Adding more consecutive harmonics strongly affects the temporal modulation of the sheath width at both electrodes in different ways, as shown in figures 1 and 4: (i) The sheath voltage increases faster on both sides due to a steeper applied voltage waveform. (ii) As $\bar{n}_{\text{sp}} < \bar{n}_{\text{sg}}$ due to the negative dc self-bias at $\theta_k = 0^\circ \forall k$, the maximum sheath width is larger at the powered electrode and the sheath expands much faster at the powered compared with the grounded electrode. (iii) Since ε strongly deviates from unity, non-linear plasma series resonance (PSR) oscillations of the RF current are self-excited during sheath collapse at the powered electrode for high values of N and enhance the electron heating via non-linear electron resonance heating (NERH) [22, 23, 67–74]. The latter two mechanisms induce an asymmetry to the spatio-temporal ionization dynamics and cause the ionization rate to be much higher at the powered compared with the grounded electrode for high values of N and for $\theta_k = 0^\circ \forall k$. Due to these mechanisms Γ_i generally increases as a function of N at low pressures and is slightly higher at the powered compared with the grounded electrode (see figure 6).

For $N = 4$ changing the phase angle, θ, affects the spatio-temporal ionization dynamics, as shown in figures 8(*a*)–(*c*). For $\theta = 0^\circ$ the ionization is dominated by sheath expansion heating enhanced by NERH at the powered electrode. The self-excitation of the PSR causes high frequency oscillations of the ionization rate at the powered electrode. This situation is reversed at $\theta = 180^\circ$, where the ionization is maximum at the grounded electrode. For an intermediate phase of $\theta = 90^\circ$, $\varepsilon \approx 1$ and no PSR oscillations are self-excited. Moreover, the oscillation of the sheaths is identical, but 180° phase shifted at both electrodes, so that the spatio-temporal ionization dynamics is symmetric. It is characterized by two separate phases of sheath expansion at each electrode within one fundamental RF period. The corresponding ionization maxima are weaker compared with the maximum at $\theta = 0^\circ, 180^\circ$. On time and space average, however, the ionization rates are similar at all phase angles, so that the ion flux remains approximately constant as a function of θ at low pressures (see figure 6(*a*) and (*c*)). The self-excitation of the PSR is also observed in terms of high frequency oscillations in the spatio-temporal plot of the electron heating rate for $\theta = 180^\circ$ shown in figure 8(*d*). The electron heating rate is calculated as the product of electron conduction current density and electric field.

3.2. *High pressure (100 Pa): γ-mode*

Figure 9(*a*) shows η as a function of θ at 100 Pa, $\phi_{\text{tot}} = 120$ V and $\gamma = 0.4$. Similar to the scenario at 3 Pa described in the previous section, the dc self-bias can be tuned effectively by adjusting θ via the EAE and adding more consecutive harmonics significantly increases the control interval of η. The increase in $|\eta|$ as a function of N for $\theta_k = 0^\circ \forall k$ is shown in figure 9(*b*). Compared with the low-pressure scenario, however, the maximum of the relative amplitude of the dc self-bias, $\bar{\eta} = \eta/\phi_{\text{tot}}$, is reduced from about 55% to 25% for $N = 4$. This is caused by the more collisional sheaths at 100 Pa compared with 3 Pa, that prevents any self-amplification of the EAE at high pressures.

Similar to the low-pressure scenario the mean ion energy can be controlled effectively at both electrodes by tuning θ for a given number of applied consecutive harmonics, as shown in figures 10(*a*) and (*c*). The control range of $\langle E_i \rangle$ is enhanced by

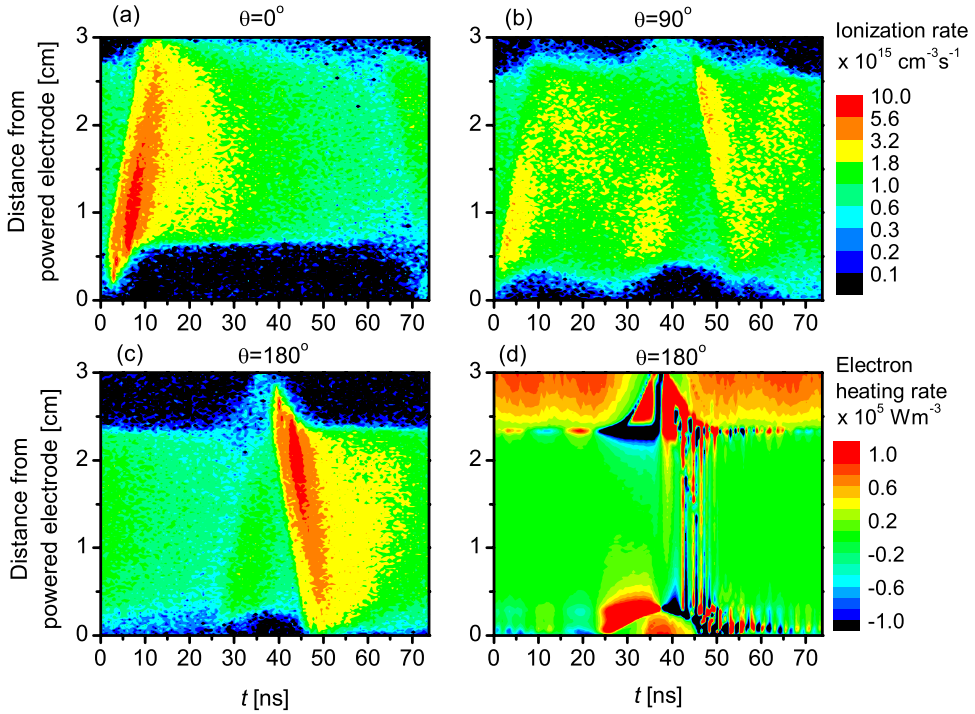

Figure 8. Spatio-temporal plots of the ionization rate in the case of $N = 4$ for different phase angles (a)–(c) and electron heating rate (d) ($p = 3$ Pa, $\phi_{\mathrm{tot}} = 800$ V, $\gamma = 0.2$). The color scales of (a)–(c) are logarithmic.

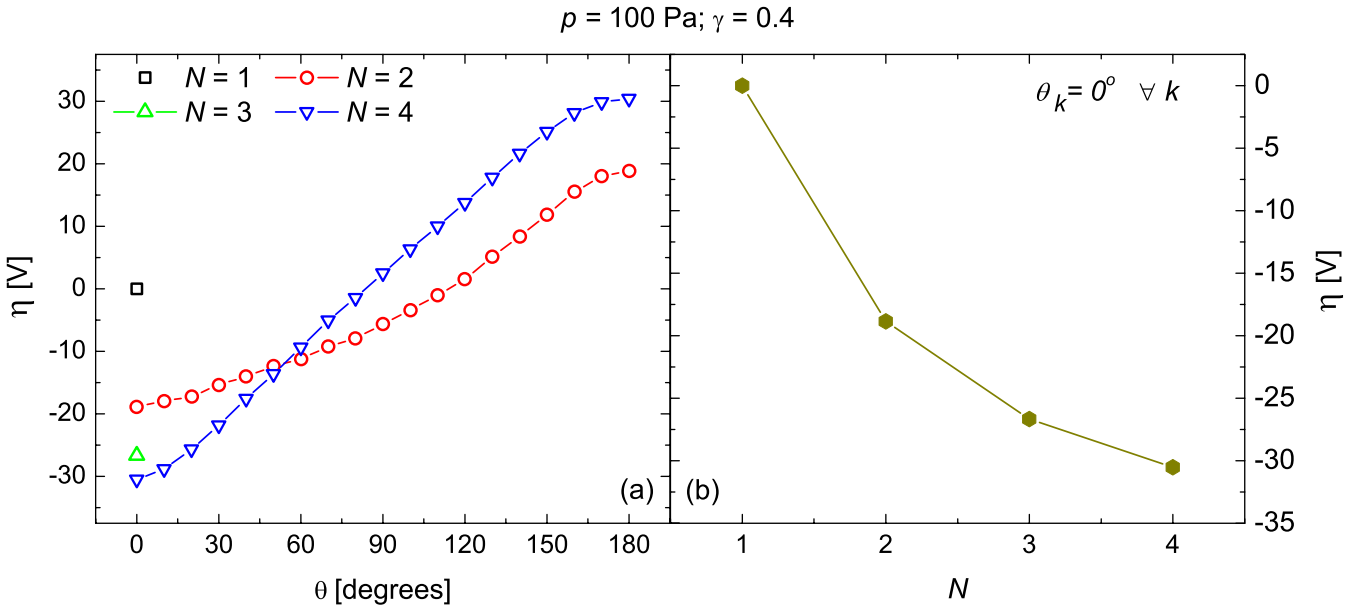

Figure 9. Dependence of the self-bias voltage, η, on (a) the identical phase angle of the even harmonics ($\theta = \theta_2 = \theta_4$, $\theta_1 = \theta_3 = 0^\circ$) for different numbers of applied harmonics, N, and (b) the number of applied harmonics for $\theta_k = 0^\circ \,\forall\, k$ ($p = 100$ Pa, $\phi_{\mathrm{tot}} = 120$ V, $\gamma = 0.4$).

adding more consecutive harmonics due to the generation of a stronger dc self-bias. $\langle E_{\mathrm{i}} \rangle$ can be changed by a factor of about 2 at both electrodes by adjusting θ. This is a much smaller control factor compared with the low pressure scenario, where the mean ion energy can be changed by a factor of about 7 due to the generation of a stronger dc self-bias caused by the self-amplification of the EAE. Moreover, the absolute values of $\langle E_{\mathrm{i}} \rangle$ are much lower at 100 Pa compared with 3 Pa due to the more collisional sheaths. For $\theta_k = 0^\circ \,\forall\, k$, figures 10$(b)$ and (d) show that $\langle E_{\mathrm{i}} \rangle$ decreases as a function of N at both electrodes. This decrease is stronger at the grounded electrode (about 60%) compared with that at the powered electrode (about 15%). Compared with the low-pressure scenario the functional dependence of $\langle E_{\mathrm{i}} \rangle$ at the powered electrode on N is completely different: while it increases as a function of N at 3 Pa (see figure 3(d)) it decreases at 100 Pa and remains approximately constant for $N \geqslant 2$. This is caused by the operation of the discharge in the γ-mode instead of the α-mode, as explained later in this section.

The ion flux is no longer constant as a function of θ for a given N, as shown in figures 11(a) and (c), but increases as a function of θ at the grounded electrode, while it decreases

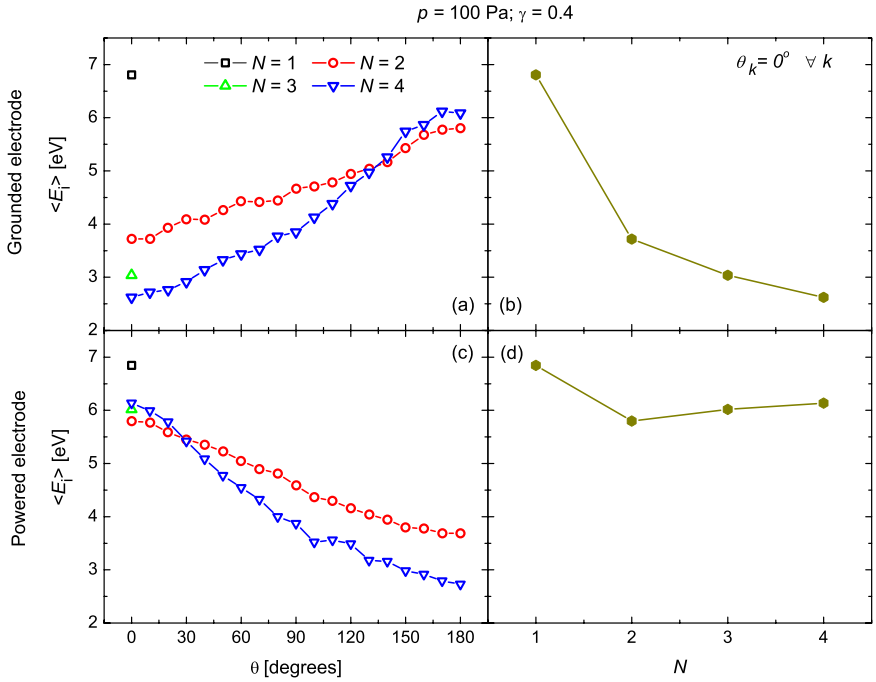

Figure 10. Mean ion energy, $\langle E_\mathrm{i}\rangle$, at the grounded and powered electrodes (top and bottom panels, respectively) as a function of $\theta = \theta_2 = \theta_4$ (left panels) for different numbers of applied harmonics, N, and as a function of N at $\theta_k = 0^\circ\,\forall\, k$ (right panels); $p = 100$ Pa, $\phi_\mathrm{tot} = 120$ V, $\gamma = 0.4$.

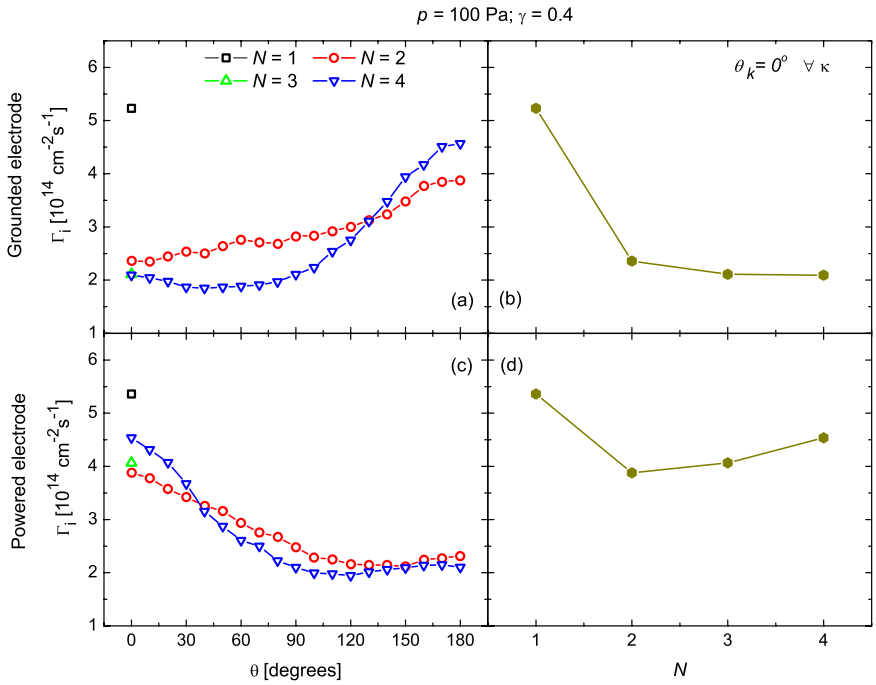

Figure 11. Ion flux, Γ_i, at the grounded and powered electrodes (top and bottom panels, respectively) as a function of $\theta = \theta_2 = \theta_4$ (left panels) for different numbers of applied harmonics, N, and as a function of N at $\theta_k = 0^\circ\,\forall\, k$ (right panels); $p = 100$ Pa, $\phi_\mathrm{tot} = 120$ V, $\gamma = 0.4$.

at the powered electrode. For $\theta_k = 0^\circ\,\forall\, k$, Γ_i decreases as a function of N at both electrodes. This decrease is stronger at the grounded electrode (about 60%) compared with that at the powered electrode (about 20%). This is completely different compared with the low-pressure scenario (see figure 6), where the ion flux increases as a function of N at both electrodes due to enhanced sheath heating. At such high pressures Γ_i and $\langle E_\mathrm{i}\rangle$ are coupled, i.e. their dependence on θ and N is similar (see figures 10 and 11), while this is not the case at low pressures (see figures 3 and 6).

These parameter trends are understood based on the analysis of the spatio-temporal ionization dynamics at 100 Pa for different numbers of applied consecutive harmonics, N, different phases and values of γ. For $\gamma = 0$, the discharge

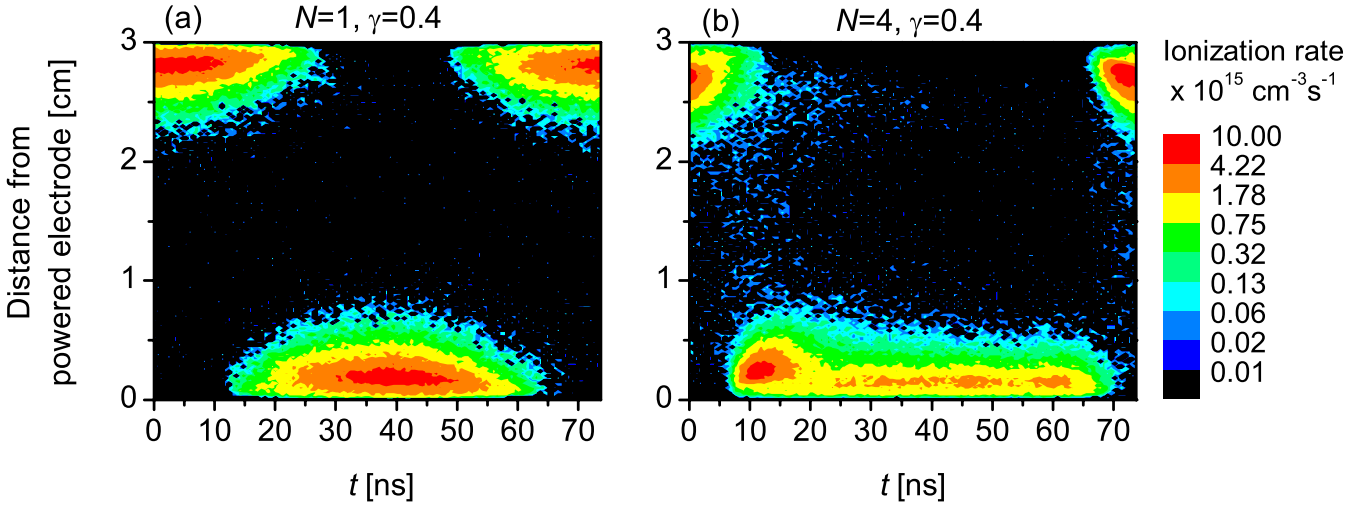

Figure 12. Spatio-temporal plots of the ionization rate for different numbers of applied harmonics ($\theta_k = 0^\circ \,\forall\, k$); $p = 100$ Pa, $\phi_{\mathrm{tot}} = 120$ V, $\gamma = 0.4$. The color scales are logarithmic.

is operated in the α-mode due to the absence of secondary electrons for all values of N. Similar to the low-pressure scenario (see figure 7) the ionization caused by sheath expansion heating is increased as a function of N and is higher at the powered compared with the grounded electrode for $\theta = 0^\circ$. However, no PSR oscillations are excited efficiently due to the strong collisional damping. Increasing γ to 0.4 induces a mode transition from the α- to the γ-mode for low values of N, i.e. $N = 1, 2$, as shown in the left plot of figure 12 for $N = 1$ as an example. In the γ-mode, maximum ionization is observed at the times of high sheath voltage at both electrodes, when γ-electrons are accelerated and multiplied most effectively inside the sheaths by collisions at high pressures. Increasing N induces another mode transition, i.e. for $N > 2$ the discharge is operated in a hybrid mode, since the sheath heating is enhanced by adding more harmonics (see the right plot of figure 12). For high values of N the sheath voltage is maximum at the powered electrode for a long fraction of the period of the fundamental driving frequency (about 50 ns for $N = 4$), while it is maximum at the grounded electrode for a much shorter time period (about 20 ns for $N = 4$). This is caused by the change in the driving voltage waveform (see figure 1). Consequently, ionization by secondary electrons is observed during a much longer fraction of the fundamental RF period at the powered compared with the grounded electrode. This causes the ion density to be higher at the powered electrode, i.e. $\bar{n}_{\mathrm{sp}} > \bar{n}_{\mathrm{sg}}$, as shown in figure 13($a$). This in turn affects the symmetry of the discharge and leads to $\varepsilon > 1$, i.e. a higher maximum sheath voltage at the grounded compared with the powered electrode according to equation (2). Therefore, the maximum of the ionization by γ-electrons is stronger at the grounded electrode. However, this is overcompensated by the longer time of ionization at the powered electrode within one fundamental RF period, so that $\bar{n}_{\mathrm{sp}} > \bar{n}_{\mathrm{sg}}$. Similar to the low-pressure scenario ε is not purely determined by $\bar{n}_{\mathrm{sp}}/\bar{n}_{\mathrm{sg}}$ for high values of N due to $(Q_{\mathrm{mg}}/Q_{\mathrm{mp}})^2 > 1$ caused by different floating potentials at both electrodes.

For $\theta_k = 0^\circ \,\forall\, k$, $\eta = |\langle\phi_{\mathrm{sg}}\rangle| - |\langle\phi_{\mathrm{sp}}\rangle|$ becomes more negative as a function of N (see figure 9(b)). This happens due to a decrease in $|\langle\phi_{\mathrm{sg}}\rangle|$, while $|\langle\phi_{\mathrm{sp}}\rangle|$ remains constant, as shown in figure 13(b). The latter is caused by the following mechanism: increasing N causes the sheath voltage to be high at the powered electrode for a longer fraction of one fundamental RF period. This would lead to an increase in $|\langle\phi_{\mathrm{sp}}\rangle|$. However, at the same time $\varepsilon = |\hat{\phi}_{\mathrm{sg}}/\hat{\phi}_{\mathrm{sp}}|$ increases as a function of N, i.e. the maximum sheath voltage at the powered electrode decreases. Both effects compensate at the powered electrode and result in a constant time-averaged sheath voltage. Despite the constant time-averaged sheath voltage the mean ion energy decreases at the powered electrode as a function of N (see figure 10(d)) due to an increase in the time-averaged sheath width at the powered electrode as a function of N, i.e. a more collisional sheath.

The ion flux is not constant as a function of θ for a fixed choice of N (see figures 11(a) and (c)) due to the change in the symmetry of the spatio-temporal ionization dynamics as a function of θ, as shown in figure 14. While the sheath voltage is high at the powered electrode for a long fraction of the fundamental RF period at $\theta = 0^\circ$, it is high at the grounded electrode for a long time at $\theta = 180^\circ$. This causes the ionization rate and the ion flux to be higher at the powered electrode at $\theta = 0^\circ$ and higher at the grounded electrode at $\theta = 180^\circ$ compared with the opposing electrode. Moreover, this dynamics causes Γ_{i} to decrease as a function of θ for $0^\circ \leqslant \theta \leqslant 180^\circ$ at the powered electrode, while it increases at the grounded electrode.

For $\theta_k = 0^\circ \,\forall\, k$, the ion flux decreases as a function of N at both electrodes, as shown in figures 11(b) and (d). At the grounded electrode this decrease is caused by the shortening of the period of high sheath voltage during one fundamental RF period, as shown in figure 12, and a decrease in the maximum sheath voltage, as shown in figure 13(c). $\hat{\phi}_{\mathrm{sg}}$ decreases as a function of N, since η becomes more negative. As the discharge is operated in γ-mode, both mechanisms lead to less ionization by secondary electrons at this electrode for high values of N and to a lower ion flux. The decrease in $|\hat{\phi}_{\mathrm{sp}}|$ as

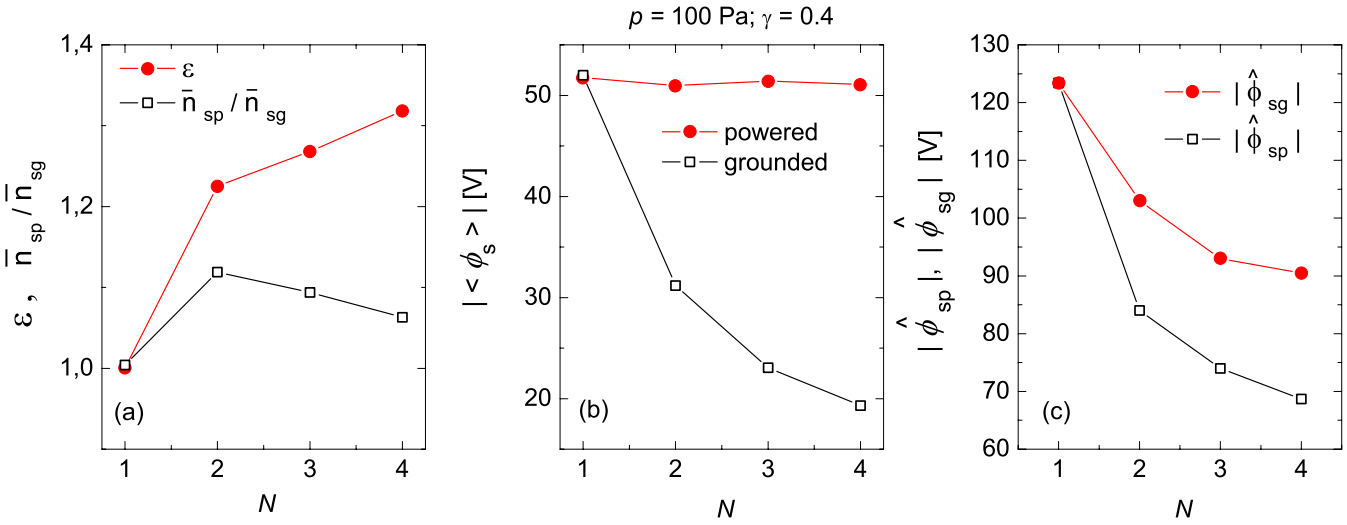

Figure 13. (*a*) Symmetry parameter and $\bar{n}_{sp}/\bar{n}_{sg}$ as a function of N. (*b*) Time-averaged sheath voltage at both electrodes as a function of N. (*c*) Absolute values of the maximum sheath voltages at both electrodes as a function of N ($\theta_k = 0^\circ\ \forall k$, $p = 100$ Pa, $\phi_{tot} = 120$ V and $\gamma = 0.4$).

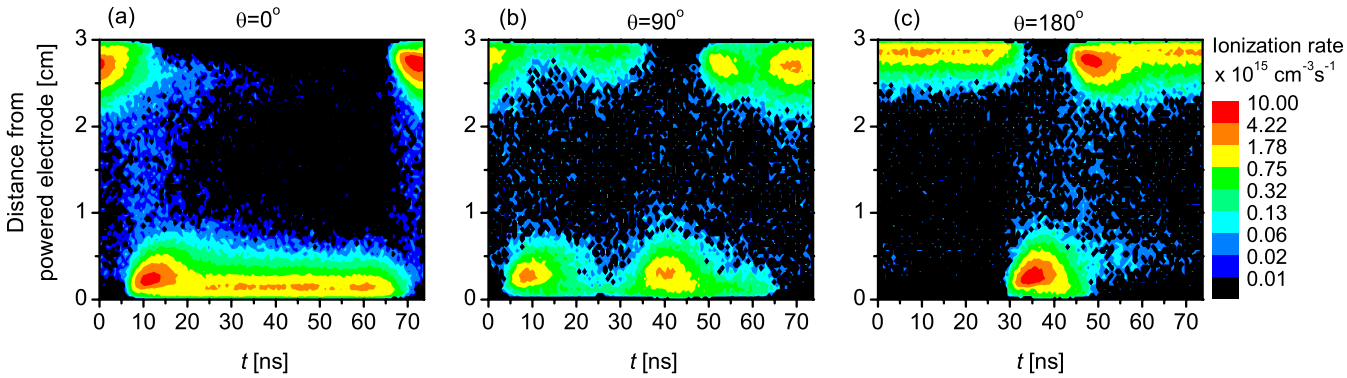

Figure 14. Spatio-temporal plots of the ionization rate for different values of θ and $N = 4$ ($p = 100$ Pa, $\phi_{tot} = 120$ V, $\gamma = 0.4$). The color scales are logarithmic.

a function of N is stronger compared with the decrease in the maximum sheath voltage at the grounded electrode. This is caused by the same mechanisms, which cause ε to be higher in multi- compared with single-frequency discharges, as shown in figure 13(*a*). This decrease in $|\hat{\phi}_{sp}|$ causes the ion flux at the powered electrode to decrease as a function of N. However, in parallel, the sheath voltage at the powered electrode is high for a longer fraction of one lf period, so that ionization by γ-electrons is efficient at this electrode for a longer time within one fundamental RF period. This partly compensates for the decrease in Γ_i as a function of N at the powered electrode and ultimately results in a weaker decrease at the powered compared with the grounded electrode, as shown in figures 11(*b*) and (*d*).

These trends of process relevant plasma parameters such as the ion flux and mean energy at the electrodes as a function of global external control parameters such as θ and N are completely different at 100 Pa compared with 3 Pa, i.e. Γ_i and $\langle E_i \rangle$ are coupled at high pressures and behave differently at low pressures at the electrodes. This difference is caused by the presence of a different electron heating mode, i.e. the γ-mode at 100 Pa and the α-mode at 3 Pa. In the γ-mode at 100 Pa, the ionization is localized at the sheaths and both the ion flux and the mean ion energy depend on the sheath voltage, while in the α-mode at 3 Pa the ionization dynamics is non-local and only $\langle E_i \rangle$ depends on the sheath voltage itself, while Γ_i and the ionization rate are determined by the temporal change in the sheath voltage.

4. Conclusions

The electron heating and ionization dynamics in capacitively coupled radio frequency argon plasmas driven by customized voltage waveforms and the effect of modifying this waveform on the ionization dynamics, the dc self-bias, η, the ion flux, Γ_i, as well as the mean ion energy, $\langle E_i \rangle$, at the electrodes were investigated by 1d3v particle-in-cell simulations. The driving voltage waveform is the sum of up to N consecutive harmonics ($N \leqslant 4$) of 13.56 MHz and can be customized by adjusting the harmonics' amplitudes and phases. Two different pressures of 3 Pa and 100 Pa were investigated to probe the collisionless low-pressure and the collisional high-pressure regimes.

We find the electrical generation of a dc self-bias, η, via the electrical asymmetry effect (EAE) to be significantly enlarged by adding more consecutive harmonics to the driving voltage waveform with specifically chosen harmonics' amplitudes according to equation (4) at a constant total voltage amplitude. η can be tuned electrically by adjusting the identical phase shift of the even harmonics, θ. In this way, the mean ion energy, $\langle E_i \rangle$, can be controlled effectively at both electrodes. The control interval for η and $\langle E_i \rangle$ is enlarged by adding more harmonics and generally larger at low pressures due to the self-amplification of the EAE.

At a low pressure (3 Pa), the discharge is operated in the α-mode, i.e. the ionization is dominated by sheath expansion heating of electrons, while the plasma is operated in the γ-mode at a high pressure (100 Pa), i.e. the ionization is dominated by secondary electrons at times of high sheath voltage. We find that the electron heating mode strongly affects the control of ion properties via the EAE.

At low pressures, the ion flux, Γ_i, remains approximately constant as a function of θ, so that the mean ion energy can be controlled separately from the ion flux at both electrodes by adjusting θ. For $\theta_k = 0^\circ \, \forall k$, the ion flux increases as a function of N at both electrodes due to enhanced sheath expansion heating of electrons caused by (i) a faster change in the applied voltage for high values of N, (ii) a larger sheath width at the powered electrode due to a lower mean ion density in this sheath, i.e. $\bar{n}_{sp} \leqslant \bar{n}_{sg}$, caused by the self-amplification of the EAE, and (iii) the excitation of plasma series resonance (PSR) oscillations of the RF current during sheath collapse at the powered electrode. The latter two mechanisms cause the ionization rate to be higher at the powered compared with the grounded electrode. $\langle E_i \rangle$ does not remain constant at either of the two electrodes.

At high pressures the presence of the γ-mode completely changes the control of ion properties via the EAE: while the mean ion energy can be tuned by adjusting θ at both electrodes, the ion flux is no longer constant as a function of the phase angle of the even harmonics. The latter is caused by a modification of the sheath voltages as a function of time at both electrodes induced by changing θ. This modification strongly affects the ionization rate at both electrodes, since it affects the acceleration and multiplication of γ-electrons inside the sheaths. Increasing the number of applied consecutive harmonics at $\theta_k = 0^\circ \, \forall k$ also affects the shape of the sheath voltages as a function of time within one fundamental RF period at both electrodes: it causes the time-averaged sheath voltage at the grounded electrode to decrease due to the generation of a more negative dc self-bias for high values of N and the shortening of the period of high sheath voltage within one fundamental RF period at this electrode. Increasing N also causes the absolute values of the maximum sheath voltages to decrease and the period of high sheath voltage within one fundamental RF period to be enlarged at the powered electrode. These effects cause $\langle E_i \rangle$ and Γ_i to decrease as a function of N at both electrodes.

Generally, these results demonstrate that a detailed fundamental understanding of the electron heating dynamics is essential for an effective optimization of process control.

Acknowledgments

We thank U Czarnetzki for helpful discussions and his support of this work. Funding has been provided by the Hungarian Fund for Scientific Research, Grant OTKA-K77653, IN 85261 and K105476.

References

[1] Lafleur T, Delattre P A, Johnson E V and Booth J P 2012 *Appl. Phys. Lett.* **101** 124104
[2] Lafleur T and Booth J P 2012 *J. Phys. D: Appl. Phys.* **45** 395203
[3] Lafleur T, Boswell R W and Booth J P 2012 *Appl. Phys. Lett.* **100** 194101
[4] Delattre P-A, Lafleur T, Johnson E and Booth J P 2013 *J. Phys. D: Appl. Phys.* **46** 235201
[5] Lieberman M A and Lichtenberg A J 2005 *Principles of Plasma Discharges and Materials Processing* 2nd edn (Hoboken NJ: Wiley Interscience)
[6] Makabe T and Petrović Z 2006 *Plasma Electronics: Applications in Microelectronic Device Fabrication* (London: Taylor and Francis)
[7] Chabert P and Braithwaite N 2011 *Physics of Radio-Frequency Plasmas* (Cambridge: Cambridge University Press)
[8] Schäfer J, Foest R, Quade A, Ohl A and Weltmann K D 2009 *Plasma Process. Polym.* **6** S519
[9] Benedikt J, Focke K, Yanguas-Gil A and von Keudell A 2006 *Appl. Phys. Lett.* **89** 251504
[10] Kong M G *et al* 2009 *New J. Phys.* **11** 115012
[11] Hemke T *et al* 2011 *J. Phys. D: Appl. Phys.* **44** 285206
[12] Hemke T *et al* 2013 *Plasma Sources Sci. Technol.* **22** 015012
[13] Waskoenig J and Gans T 2010 *Appl. Phys. Lett.* **96** 181501
[14] O'Neill C, Waskoenig J and Gans T 2012 *Appl. Phys. Lett.* **101** 154107
[15] O'Neill C, Waskoenig J and Gans T 2011 *IEEE Trans. Plasma Sci.* **39** 2588
[16] Lieberman M A 1988 *IEEE Trans. Plasma Sci.* **16** 638
[17] Lieberman M A and Godyak V A 1998 *IEEE Trans. Plasma Sci.* **26** 955
[18] Surendra M and Graves D B 1991 *Phys. Rev. Lett.* **66** 1469
[19] Turner M M 1995 *Phys. Rev. Lett.* **75** 1312
[20] Gozadinos G, Turner M M and Vender D 2001 *Phys. Rev. Lett.* **87** 135004
[21] Kaganovich I D 2002 *Phys. Rev. Lett.* **89** 265006
[22] Mussenbrock T and Brinkmann R P 2006 *Appl. Phys. Lett.* **88** 151503
[23] Schulze J *et al* 2007 *IOP Conf. Ser.* **86** 012010
[24] Liu Y X *et al* 2011 *Phys. Rev. Lett.* **107** 055002
[25] Liu Y X *et al* 2012 *Plasma Sources Sci. Technol.* **21** 035010
[26] Liu Y X *et al* 2012 *Appl. Phys. Lett.* **101** 114101
[27] Liu Y X *et al* 2013 *Plasma Sources Sci. Technol.* **22** 025012
[28] Belenguer P and Boeuf J P 1990 *Phys. Rev.* A **41** 4447
[29] Schulze J, Donkó Z, Schüngel E and Czarnetzki U 2011 *Plasma Sources Sci. Technol.* **20** 045007
[30] O'Connell D, Gans T, Semmler E and Awakowicz P 2008 *Appl. Phys. Lett.* **93** 081502
[31] Schulze J *et al* 2011 *Phys. Rev. Lett.* **107** 275001
[32] Schüngel E, Mohr S, Iwashita S, Schulze J and Czarnetzki U 2013 *J. Phys. D: Appl. Phys.* **46** 175205
[33] Boeuf J P and Belenguer Ph 1992 *J. Appl. Phys.* **71** 4751
[34] Gogolides E, Nicolai J P and Sawin H H 1989 *J. Vac. Sci. Technol.* A **7** 1001
[35] Gogolides E and Sawin H H 1992 *J. Appl. Phys.* **72** 3971
[36] Yan M, Bogaerts A, Gijbels R and Goedheer W J 2000 *J. Appl. Phys.* **87** 3628
[37] Belenguer Ph *et al* 1992 *Phys. Rev.* A **46** 7923

[38] Yan M, Bogaerts A, Goedheer W J and Gijbels R 2000 *Plasma Sources Sci. Technol.* **9** 583
[39] Wang S B and Wendt A E 2000 *J. Appl. Phys.* **88** 643
[40] Patterson M M, Chu H-Y and Wendt A E 2007 *Plasma Sources Sci. Technol.* **16** 257
[41] Baloniak T, Reuter R and von Keudell A 2010 *J. Phys. D: Appl. Phys.* **43** 335201
[42] Donkó Z *et al* 2012 *Plasma Phys. Control. Fusion* **54** 124003
[43] Boyle P C, Ellingboe A R and Turner M M 2004 *Plasma Sources Sci. Technol.* **13** 493–503
[44] Boyle P C, Ellingboe A R and Turner M M 2004 *J. Phys. D: Appl. Phys.* **37** 697
[45] Olevanov M, Proshina O, Rhakhimova T and Voloshin D 2008 *Phys. Rev.* E **78** 026404
[46] Gans T *et al* 2006 *Appl. Phys. Lett.* **89** 261502
[47] Turner M M and Chabert P 2006 *Phys. Rev. Lett.* **96** 261502
[48] Booth J P, Curley G, Marić D and Chabert P 2010 *Plasma Sources Sci. Technol.* **19** 015005
[49] Heil B G *et al* 2008 *IEEE Trans. Plasma Sci.* **36** 1404
[50] Heil B G, Czarnetzki U, Brinkmann R P and Mussenbrock T 2008 *J. Phys. D: Appl. Phys.* **41** 165202
[51] Czarnetzki U, Schulze J, Schüngel E and Donkó Z 2011 *Plasma Sources Sci. Technol.* **20** 024010
[52] Schulze J, Schüngel E, Donkó Z and Czarnetzki U 2010 *Plasma Sources Sci. Technol.* **19** 045028
[53] Longo S and Diomede P 2009 *Plasma Process. Polym.* **6** 370
[54] Schulze J, Schüngel E, Donko Z and Czarnetzki U 2011 *Plasma Sources Sci. Technol.* **20** 015017
[55] Korolov I, Donko Z, Czarnetzki U and Schulze J 2012 *J. Phys. D: Appl. Phys.* **45** 465205
[56] Johnson E V *et al* 2012 *J. Non-Cryst. Solids* **358** 1974
[57] Johnson E V, Delattre P A and Booth J P 2012 *Appl. Phys. Lett.* **100** 133504
[58] Johnson E V, Verbeke T, Vanel J-C and Booth J P 2010 *J. Phys. D: Appl. Phys.* **43** 412001
[59] Hrunski D *et al* 2013 *Vacuum* **87** 114
[60] Bienholz S, Bibinov N and Awakowicz P 2013 *J. Phys. D: Appl. Phys.* **46** 084010
[61] Phelps A V and Petrović Z Lj 1999 *Plasma Sources Sci. Technol.* **8** R21
[62] Phelps A V 1994 *J. Appl. Phys.* **76** 747
[63] Phelps A V http://jilawww.colorado.edu/∼avp/collision_data/ unpublished
[64] Kollath R 1956 *Encyclopedia of Physics* vol XXI, ed S Flügge (Berlin: Springer) p 264
[65] Donkó Z and Petrović Z Lj 2006 *J. Phys.: Conf. Ser.* **86** 012011
[66] Brinkmann R P 2007 *J. Appl. Phys.* **102** 093302
[67] Czarnetzki U, Mussenbrock T and Brinkmann R P 2006 *Phys. Plasmas* **13** 123503
[68] Mussenbrock T and Brinkmann R P 2007 *Plasma Sources Sci. Technol.* **16** 377
[69] Lieberman M A *et al* 2008 *Phys. Plasmas* **15** 063505
[70] Mussenbrock T *et al* 2008 *Phys. Rev. Lett.* **101** 085004
[71] Ziegler D, Mussenbrock T and Brinkmann R P 2008 *Plasma Sources Sci. Technol.* **17** 045011
[72] Boffard J B, Jung R O, Lin C C, Aneskavich L E and Wendt A E 2012 *J. Phys. D: Appl. Phys.* **45** 382001
[73] Donkó Z, Schulze J, Czarnetzki U and Luggenhölscher D 2009 *Appl. Phys. Lett.* **94** 131501
[74] Bora B, Bhuyan H, Favre M, Wyndham E and Chuaqui H 2012 *Appl. Phys. Lett.* **100** 094103